A Flight-Calibrated Methodology for Determination of Cassini Thruster On-Times for Reaction Wheel Biases

Siamak Sarani*

Jet Propulsion Laboratory
4800 Oak Grove Drive, Pasadena, CA 91109-8099
California Institute of Technology

This paper describes a methodology for accurate and flight-calibrated determination of the on-times of the Cassini spacecraft Reaction Control System (RCS) thrusters, without any form of dynamic simulation, for the reaction wheel biases. The hydrazine usage and the ΔV vector in body frame are also computed from the respective thruster on-times. The Cassini spacecraft, the largest and most complex interplanetary spacecraft ever built, continues to undertake ambitious and unique scientific observations of planet Saturn, Titan, Enceladus, and other moons of Saturn. In order to maintain a stable attitude during the course of its mission, this three-axis stabilized spacecraft uses two different control systems: the RCS and the reaction wheel assembly control system. The RCS is used to execute a commanded spacecraft slew, to maintain three-axis attitude control, control spacecraft's attitude while performing science observations with coarse pointing requirements, e.g. during targeted low-altitude Titan and Enceladus flybys, bias the momentum of reaction wheels, and to perform RCS-based orbit trim maneuvers. The use of RCS often imparts undesired ΔV on the spacecraft. The Cassini navigation team requires accurate predictions of the ΔV in spacecraft coordinates and inertial frame resulting from slews using RCS thrusters and more importantly from reaction wheel bias events. It is crucial for the Cassini spacecraft attitude control and navigation teams to be able to, quickly but accurately, predict the hydrazine usage and ΔV for various reaction wheel bias events without actually having to spend time and resources simulating the event in flight software-based dynamic simulation or hardware-in-the-loop simulation environments. The methodology described in this paper, and the ground software developed thereof, are designed to provide just that. This methodology assumes a priori knowledge of thrust magnitudes and thruster pulse rise and tail-off time constants for eight individual attitude control thrusters, the spacecraft's wet mass and its center of mass location, and a few other key parameters.

Acronyms

AACS	AACS Attitude and Articulation Control System
AU	Astronomical Unit (=149,597,870.7 km)
c.m.	Center of Mass
db	Dead-band
EME	Earth Mean Equatorial
ESA	European Space Agency
FSDS	Flight Software Development System
FSW	Flight Software
GSW	Ground Software
Ibit	Minimum Impulse Bit
IRU	Inertial Reference Unit
Isp	Specific Impulse
JPL	Jet Propulsion Laboratory

* Senior Member of Technical Staff, Guidance and Control Section, Jet Propulsion Laboratory, Mail Stop 230-104, 4800 Oak Grove Drive, Pasadena, California 91109-8099, USA. Siamak.Sarani@jpl.nasa.gov

MTA	Monopropellant Tank Assembly
PMS	Propulsion Module Subsystem
RCS	Reaction Control System
RTI	Real-Time Interrupt
RWA	Reaction Wheel Assembly
SRU	Stellar Reference Unit
VDE	Valve Drive Electronics

Table of Contents

Section Page

Acronyms 1
I. Cassini: Six Years at Saturn and Going Strong 2
II. Monopropellant Hydrazine Propulsion System 3
III. Cassini Reaction Control System 4
IV. Cassini Reaction Wheel Assembly Manger 8
V. Thruster On-Time Determination for Ideal Thrusters 12
VI. Flight-Calibrated Thruster On-Times 14
VII. ΔV and Propellant Consumption Determination 17
VIII. Comparing Results for Eight Reaction Wheel Bias Events 18
IX. Summary and Conclusions 22
Acknowledgements 22
References 22

I. Cassini: Six Years at Saturn and Going Strong

The Cassini-Huygens mission is managed by the Jet Propulsion Laboratory, a division of the California Institute of Technology in Pasadena. This highly visible and successful mission has been and continues to be an international endeavor involving the NASA, the European Space Agency (ESA), and multiple academic and industrial partners.[1,2,3] The Cassini spacecraft (Fig. 1) is the most sophisticated spacecraft ever built and sent to explore our solar system and continues to undertake a series of ambitious and unique scientific observations of planet Saturn, Titan, and other Cronian satellites. It continues to remain in excellent health in the harsh and unfriendly environment of space at a distance of ~9.5 AU from the sun. The Cassini mission has successfully completed its 4-year prime mission and is just about to end its 2-year Equinox extended mission. After the completion of the Equinox mission around September 2010, Cassini will start its seven-year Solstice extended mission.[1,2,3]

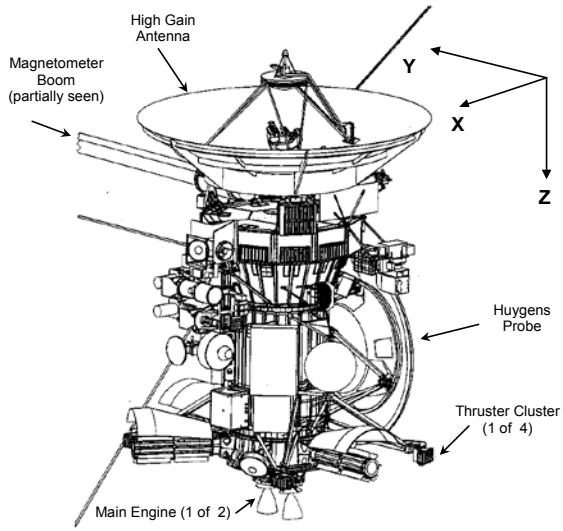

Fig. 1 Cassini spacecraft. One of the four thruster clusters can be seen in this view of the spacecraft.

Cassini's Attitude and Articulation Control System (AACS) estimates and controls the spacecraft attitude and executes ground-commanded spacecraft velocity changes. It points the spacecraft's science instruments and communication antennas towards targets of interest. Cassini is a three-axis stabilized spacecraft and in order to maintain a stable attitude during the course of its mission, it uses two different control systems: the Reaction Control System (RCS) and the Reaction Wheel Assembly (RWA) control system.[8]

II. Monopropellant Hydrazine Propulsion System

A monopropellant propulsion system (Fig. 2.a) generates hot, high velocity gases by decomposing hydrazine (N_2H_4) as a single chemical, a monopropellant. Hydrazine is injected into a catalyst bed, where it chemically decomposes to expel ammonia, nitrogen, and hydrogen at high temperatures and velocities. The resulting hot gases are expelled through a converging-diverging nozzle generating thrust in opposite direction. The gas temperature is in the 1200 C range.[4]

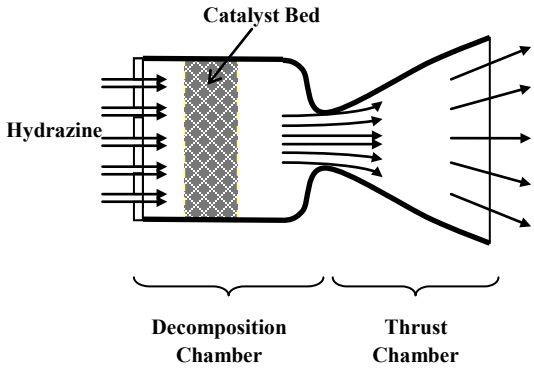

(a)

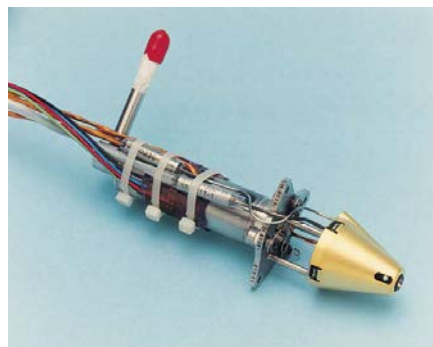

(b)

Fig. 2 (a) Diagram of monopropellant propulsion system. (b) One of Cassini's 1-N monopropellant hydrazine thruster (*courtesy Aerojet, a GenCorp, Inc.)*

First, the hydrazine decomposes to ammonia. This reaction is exothermic and the adiabatic flame temperature is ~1400 C. The ammonia further decomposes into hydrogen and nitrogen. This reaction is endothermic and leads to a reduction in flame temperature and specific impulse. Attitude control applications of monopropellant hydrazine engines require operation over wide ranges of duty cycles and pulse widths and for such uses, the pulsing specific impulse and *minimum impulse bit* (Ibit) are both very important.[4] Also, the valve performance is an integral part of the thruster performance during pulsing.

The Cassini Propulsion Module Subsystem (PMS) is by far the most complex interplanetary propulsion system ever flown. The monopropellant propulsion system for Cassini is of the blow-down type, consisting of a single hydrazine tank and sixteen (eight primary and eight backup) hydrazine thrusters with a thrust range of 0.5 to 1.0 N, and a helium recharge tank.[5] Fig. 2.b depicts one of Cassini 's 1-N (0.2-lbf) monopropellant hydrazine thrusters. The two branches of the RCS thrusters are completely redundant, and the prime branch is designated A-Branch and the back-up branch is designated B-Branch. In each of the RCS thrusters, there is a catalyst bed of platinum/iridium, on an aluminum substrate, with three parallel electric heaters on the surface. The heaters improve the thruster chemical reaction transients and prevent damage to the catalyst bed. Thruster firings using a thruster with a catalyst that is not heated (cold start) cause damage to the catalyst and the cold start count per thruster will be limited.[5]

The RCS thrusters are fed from a tank initially containing 132 kg of monopropellant hydrazine at the launch configuration. As characterized by the blow-down system, the hydrazine tank pressure decays slowly with time as hydrazine is depleted through thruster firings.[4,5] The hydrazine propellant tank output is fed using surface tension vanes. The fuel flows from the tank through the fuel lines, latch valves, filters, and solenoid valves to the thrusters. The latch valves are used to open or close branches. They are solenoid valves with separate open and close coils, which are spring loaded and nominally closed. The valves of the RCS thrusters are driven by the Valve Drive Electronics (VDE). The AACS Flight Software (FSW) controls the RCS thrusters directly through individual thruster on/off commands applied with timing delays. Although the software can only schedule thruster valve commands every computational cycle (= 125 ms), thruster on-times can be commanded to be as short as 7 ms and as long as 125 ms.[6,8]

The thrust magnitudes of the operating RCS thrusters have been changing and will continue to change throughout the Cassini mission. At launch (October 15, 1997), the thrust magnitude was about 0.97 N. By the time of Saturn Orbit Insertion (June 30, 2004), the thrust magnitude had decayed to 0.75 N. By the time of Probe relay (January 14, 2005), the thrust magnitude was 0.69 N. The Monopropellant Tank Assembly (MTA) of Cassini was recharged on April 10, 2006, and this caused an increase of approximately 50% in thrust magnitudes of the primary and backup RCS thrusters. This recharge utilized the single helium pressurant recharge tank. On March 12, 2009, Cassini successfully swapped to the backup RCS thrusters. Shortly after the swap, the nominal operation of the B-branch RCS thrusters was verified by Cassini Attitude and Articulation Control Subsystem (AACS) team.[1,2,15]

III. Cassini Reaction Control System

The reaction control system (RCS) of Cassini is responsible for maintaining the three-axis attitude control for the spacecraft, when the reaction wheels are not operating, and perform many other unique functions. The RCS has been used in the past to perform a full sky sun acquisition following separation from the launch vehicle, de-tumble the spacecraft after the upper stage separation and after the Huygens probe release, perform RCS-based trajectory correction maneuvers (achieved by firing four Z-facing thrusters), and hold the spacecraft with optimal limit cycle control during the entire cruise. The RCS is used to execute a commanded spacecraft slew, to maintain 3-axis attitude control, control spacecraft's attitude while performing science observations with coarse pointing requirements, e.g. during targeted low-altitude Titan and Enceladus flybys, bias the momentum of reaction wheels, and perform RCS-based orbit trim maneuvers. The RCS also enables Cassini to do a lot of large angle, quick (0.75 °/sec) angular maneuvers.[6,8]

Cassini's thrusters have rich heritage from the Voyager program.[5] The RCS system consists of sixteen (eight primary or A-branch and eight backup or B-branch) hydrazine thrusters, placed in four clusters. The four thruster clusters are mounted via tripods to the propulsion module, at the corners of a rectangle parallel to the spacecraft X-Y plane.[1,5] The thrusters are mounted in approximately collocated pairs for redundancy. Each cluster has a pair of thrusters, which thrust in -Z direction (X and Y axis control thrusters) and another pair, which thrust in the ±Y direction (Z axis control thrusters). A diagram of thruster locations and thrust directions is depicted in Fig. 3. With reference to this figure, we see that to slew about the positive Z axis of the spacecraft, or for pointing control about +Z, one must fire both the Y_2 and Y_4 thrusters simultaneously. Thrusts generated by these firings will almost cancel each other, and the ΔV imparted on the spacecraft will be negligible. Similarly, to slew about the negative Z axis of the spacecraft, or for pointing control about –Z axis, one must fire both the Y_1 and Y_3 thrusters simultaneously. Again, the ΔV imparted on the spacecraft will be small. On the other hand, a slew about either the ±X axis or ±Y axis or pointing controls about the spacecraft's X and Y axes will involve firings of the Z-facing thrusters. Since these Z-facing thrusters all point in the same direction, slewing the spacecraft about either the X or Y-axis will generate unwanted ΔV on the spacecraft that must be predicted.[1,2,8]

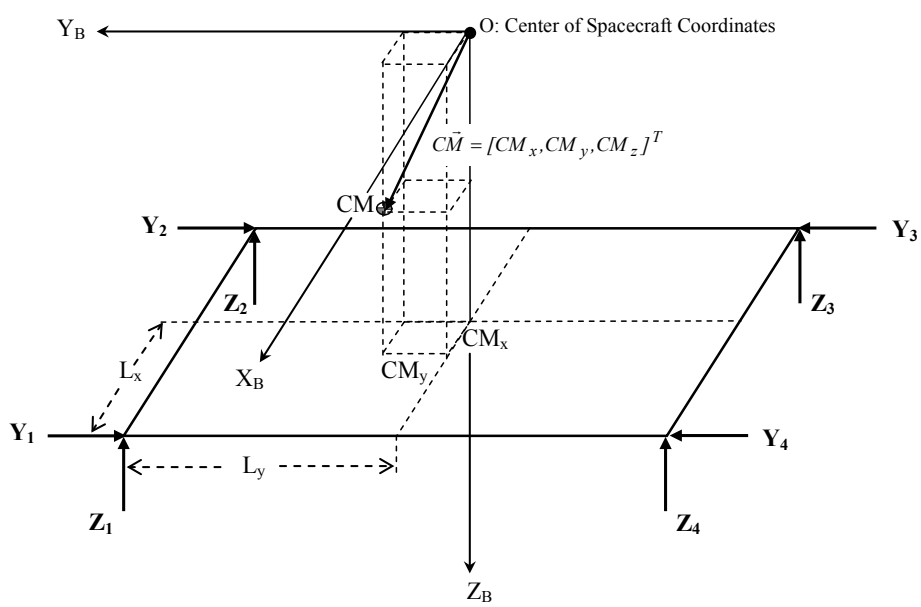

Fig. 3 Cassini RCS thruster configuration. Depicted center of mass location is for current configuration.

Table 1 captures the RCS thrust directions. The X-axis control authority[14] with B-branch thrusters is a few percent larger than that generated by A-branch thrusters. The Y-axis and Z-axis control authorities are identical.

Table 1 RCS thruster thrust directions

RCS Branch	RCS Thrusters	Thrust Direction		
		X	Y	Z
A-Branch	Z_{1A}	0	0	-1
	Z_{2A}	0	0	-1
	Z_{3A}	0	0	-1
	Z_{4A}	0	0	-1
	Y_{1A}	0	-1	0
	Y_{2A}	0	-1	0
	Y_{3A}	0	+1	0
	Y_{4A}	0	+1	0
B-Branch	Z_{1B}	0	0	-1
	Z_{2B}	0	0	-1
	Z_{3B}	0	0	-1
	Z_{4B}	0	0	-1
	Y_{1B}	0	-1	0
	Y_{2B}	0	-1	0
	Y_{3B}	0	+1	0
	Y_{4B}	0	+1	0

The RCS controller consists of a classical bang-off-bang controller, a dead-band, and a set of thruster mapping logic (see Table 2).[6,10] It takes both position and rate error signals and processes them through these three components. Fig. 4 captures the RCS controller architecture. The RCS controller stabilizes the spacecraft's inertial attitude dynamics by feeding back the current spacecraft attitude profiles (position and rate) using the on-board Stellar Reference Unit (SRU) and/or the 3-axis Inertial Reference Unit (IRU). These can be carried out separately or together depending on the operation mode.[6,10] An attitude estimator subsequently processes the on-board spacecraft attitudes and feeds back its best attitude estimations. The RCS then compares the commanded spacecraft attitude profiles with this on-board knowledge to create a 3-axis error vector. This error vector is then passed onto the RCS controller to decide the proper control actions. The additional rate feedback provides damping to the overall system. The RCS controller algorithms are designed to use the error signals, which are the weighted sums of per-axis attitude and rate errors, to control thruster firings while incorporating an adaptive or self-tuning feature to produce one-sided limit cycles in the presence of small environmental torque.[7,10] The AACS FSW controls the RCS thrusters directly through individual thruster on/off commands applied with small duration pulses and timing delays. The timing resolution allows for precise control of the thruster on periods with a minimal cost to the AACS computing power.

As seen in Fig. 4, the linear part of the RCS control law is simply a switching function of the following form $u = -(e_\theta + ke_\omega)$, where the switching line on phase plane is a linear equation with slope $-1/k$.[6,8] Rate saturation limits and their relative dead-band can be implemented as limited error position signals with limits clamped at 0.75 °/sec, the maximum allowable rate, multiplied by the rate gain k.[6,7,9] Then, the total error to be evaluated against the dead-band is the sum of "clamped" error position and rate error times the rate gain. A small dead-band is also assigned to the RCS controller to avoid chattering. The duration of burn for each thruster is defined by the control designer to set an upper bound on the overall RCS duty cycle.[6] The current value is set to 1 RTI = 125 ms, where RTI is the Real-Time Interrupt of Cassini AACS FSW.

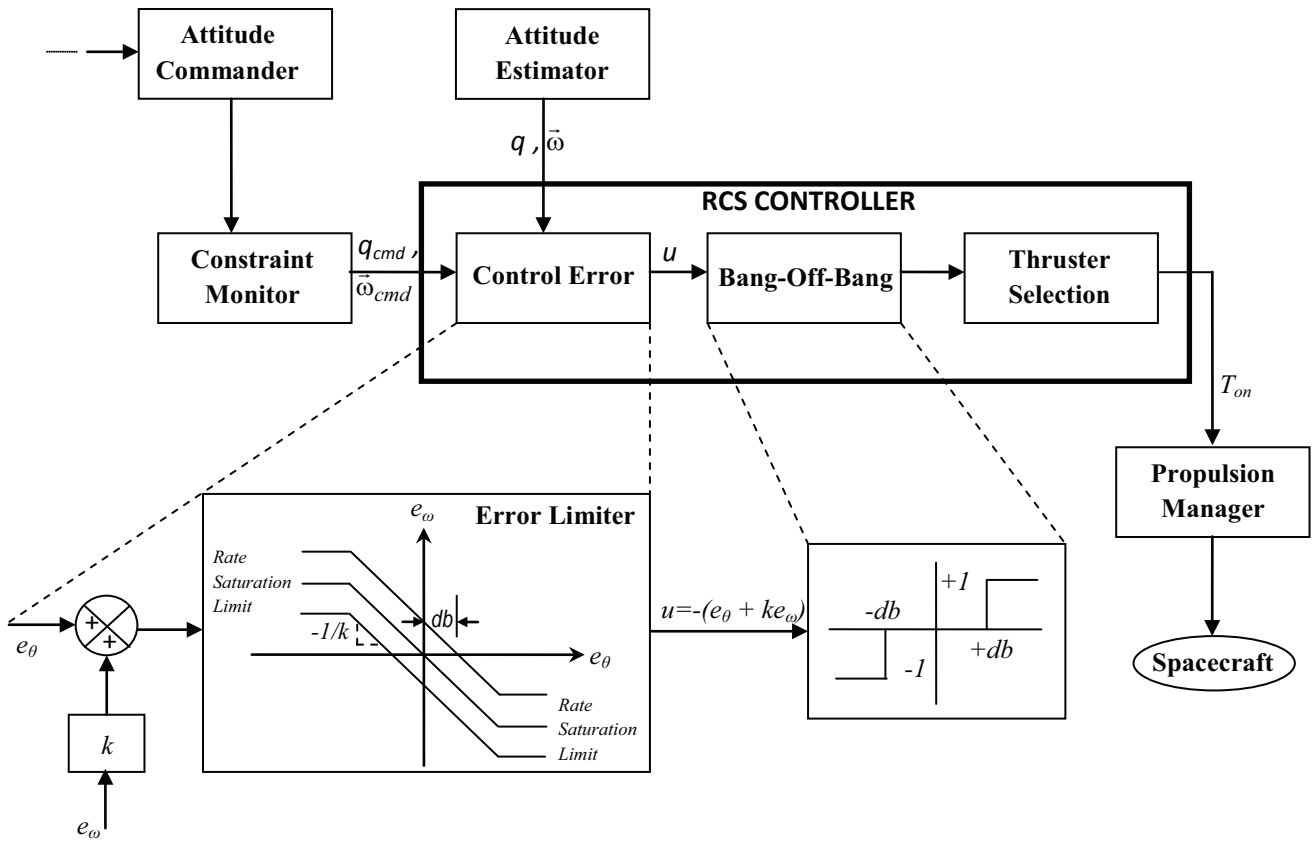

Fig. 4 RCS controller architecture.

Thruster mapping logic is also part of the RCS controller. It is depicted in Table 2.

Table 2 RCS thruster mapping

Thruster Mapping		Z-Facing Thrusters				Y-Facing Thrusters			
		Z_1	Z_2	Z_3	Z_4	Y_1	Y_2	Y_3	Y_4
X	+			×	×				
	-	×	×						
Y	+	×			×				
	-		×	×					
Z	+						×		×
	-					×		×	
• If Z_1 and Z_3 are both on, then Z_1 and Z_3 firings are inhibited • If Z_2 and Z_4 are both on, then Z_2 are Z_4 firings are inhibited									

RCS attitude control algorithm can operate in four different modes:[6]

(i) Idle Mode: No control action is required, i.e., no thrusters are fired. This mode is used immediately before and after the Probe release and during spacecraft launch and deployment.

(ii) RCS Rate Mode: This mode is used to bring the spacecraft to a specified rate from an arbitrary initial rate without position feedback signals, e.g., to stop spacecraft launch tip-off rate, de-tumble after Probe release, or fault protection reaction to a tumbling spacecraft.

(iii) Position and Rate at High Rate Mode: This mode is used during normal operations such as turn/hold, Titan flyby, sun search, RWA bias, etc.

(iv) Position and Rate at Low Rate Mode: This mode is used during cruise operation. Optimal limit cycle of position error trajectories are desired to save thruster cycles.

The switching between high rate and low rate RCS controls is implemented as follows: the switching from high rate to low rate is done if both rate command and rate error signals are persistently low for 10 min. On the other hand, switching from low rate to high rate is performed if the rate command is large, the rate error is persistently high for 3 seconds, or if there are 3 consecutive nonzero thruster commands larger than 80 msec.[6,10]

While on RCS control, the spacecraft's attitude control errors are commanded via an attitude dead-band set-up command. The three arguments of this command provide the FSW with the magnitudes of the one-sided dead-band about the spacecraft's X, Y, and Z-axis. At times when accurate pointing was not needed, AACS used dead-band of [20, 20, 20] mrad in order to save both hydrazine and thruster on/off cycle. On the other hand, the attitude control dead-band is tightened during such events as the RWA bias to [2, 2, 2] mrad.

The walking dead-band is a special feature that has been incorporated in RCS control. It was added to avoid an undesirable phenomenon called double pulsing, which also wastes both hydrazine and thruster on/off cycle. The walking dead-band feature is activated whenever dead-band crossing occurs.[8] The dead-band is increased to a value that is greater than that commanded by the ground operators by one or more small steps. Representative walking dead-band step size is 0.2 mrad, and a maximum of 5 steps are allowed.[8] These walking dead-band parameters could be changed via an AACS command. Another important design consideration of the Cassini RCS controller is related to the possible control-structure interactions between thruster firings and the 0.7-Hz magnetometer boom especially during a low altitude Titan flyby.[8,9] To avoid these undesirable interactions, 2nd order notch filters (with a notch frequency of 0.7 Hz) are used to filter both the attitude and attitude rate control error signals. The filtered signals are then combined to form the error signal for the RCS controller. The bandwidth of the RCS attitude controller is selected to be 0.15 Hz, which is significantly higher than the low-g bi-propellant slosh appendage modes (2-4 mHz at 50% tank fill fraction). The gain and phase margins of the RCS controller are 18 dB and 25°, respectively.

Each RCS thruster pulse is modeled according to Fig. 5. The four parameters F_{thr}, Δ, t_R, and t_T are the steady-state thrust, the commanded pulse width, the exponential rise-time constant, and the exponential tail-off time constant, respectively. The residual impulse (I_{res}) for a single thruster pulse of width Δ equals:[1,2,3]

$$\begin{aligned} I_{res}(\Delta) &= \int_0^{\Delta} F_{thr}(1-e^{-t/t_R})dt + \int_{\Delta}^{\infty} F_{thr}(1-e^{-\Delta/t_R})e^{-(t-\Delta)/t_T}dt - F_{thr}\Delta \\ &= F_{thr}(t_T - t_R)(1-e^{-\Delta/t_R}) \approx F_{thr}(t_T - t_R) \end{aligned} \tag{1}$$

The commanded impulse associated with a single thruster pulse with pulse width of Δ, or the impulse generated by an "ideal" thruster with zero rise and tail-off time constants, , is $F_{thr}\Delta$ and is represented in Fig. 5 by the shaded area. The solid thick line indicates the actual pulse. The residual impulse is simply the difference between the area under the curve of the actual pulse and that of the ideal pulse. During the RWA bias event, the RCS thruster pulses are typically 125 or 250 ms wide. For thruster pulse width of 125 ms (or 250 ms), the factor $1-e^{-\Delta/t_R} \approx 0.998$ in Eq. 1, and hence assuming $I_{res}(\Delta) \approx F_{thr}(t_T - t_R)$ is a sufficiently good assumption.

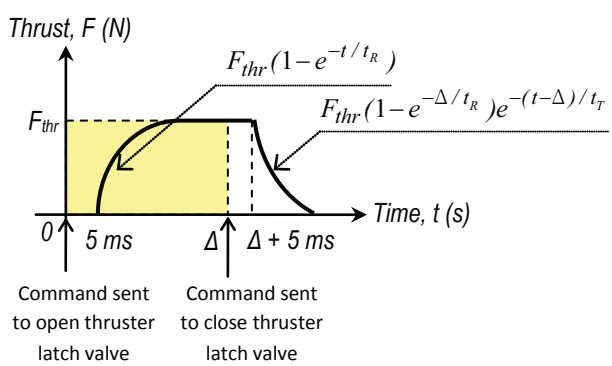

Fig. 5 RCS Thruster pulse model (not to scale).

For A-branch thrusters the typical values for t_R and t_T are 20 ms and 43-65 ms, respectively. For B-branch thrusters the typical values for t_R and t_T are 20 ms and ~31 ms, respectively. The rise time remains constant, while the tail-off time varies with time. The tail-off time was about 65 ms before the MTA recharge. It dropped to 43 ms after the recharge. Since then, it started growing gradually to 48 ms. The rise time constant of the thruster pulses remained unchanged at 20 ms. After swapping to the B-branch, the tail-off time constant shortened to ~31 msec

because B-branch thrusters were pristine at that time. Once again, the rise time constant remained unchanged after the swap. Since the swap event, the tail-off time constant has grown, but not by much.

The event of focus in this paper is the momentum management of the reaction wheels under RCS control, i.e. the RWA bias. A representative reaction wheel biasing is carried out as follows. The spacecraft is Earth-pointed and is on thruster control, with dead-bands of [2, 2, 2] mrad. After being powered on, the reaction wheels are spun up to attain a set of pre-selected spin rates. In so doing, the dc motors of the RWAs impart equal and opposite torque on the spacecraft.[8] Thrusters are then fired to maintain the spacecraft's attitude in the presence of these disturbance torques. In the worst case, a reaction wheel biasing will take less than 20 minutes to complete. The RWA manager enforces RWA speed control to bias the wheels, while RCS is in control for attitude hold and pointing.[6]

The Cassini AACS team simulates the RWA bias events using a simulation environment called The FSW Development System (FSDS). The FSDS is a high-fidelity test-bed that is used to perform guidance, control, and fault protection simulations. It is a closed-loop environment using the latest version of the AACS FSW.[2,3,12] For any Cassini events of interest, FSDS is a faster-than-real-time simulation environment of choice for AACS team and has been used extensively to develop and validate AACS FSW loads, perform various testing of critical events for Cassini, e.g. the launch, Saturn orbit insertion, Probe release, and Probe relay tracking, check first-time events, and investigate flight anomalies. Spacecraft dynamics model within FSDS includes a rigid body plus system flexibilities such as the Magnetometer boom and Radio and Plasma Wave Science antennas, and propellant sloshing.[2,3,12]

The use of the RCS often imparts undesired ΔV on the spacecraft. The Cassini navigation requires that the spacecraft system provides predictions of the ΔV in spacecraft coordinates resulting from a turn using RCS thrusters and a reaction wheel bias. The navigation requirement states that the prediction of these ΔV effects on the spacecraft shall be accurate to 3% of nominal value (3σ) in each component.

It is crucial for Cassini uplink and navigation teams to be able to quickly, but accurately, predict the hydrazine usage and ΔV for key RCS-controlled Cassini events, such as the reaction wheel biases and spacecraft single-axis or multi-axis slews, without actually having to spend time and resources simulating the event in FSDS or hardware-in-the-loop simulation environments. This paper explains a methodology for accurate and flight-calibrated prediction of the RCS thruster on-times, without any form of simulation, for various reaction wheel bias events. The hydrazine usage and the ΔV vector are also computed from the thruster on-times. This methodology assumes a priori set of thrust magnitude and thruster pulse rise and tail time constants for individual RCS thrusters.

IV. Cassini Reaction Wheel Assembly Manager

Cassini has a set of three fixed reaction wheels that are oriented such that their spin axes make equal angles with the spacecraft's Z-axis. Each wheel is considered a reaction wheel assembly (RWA), and the three fixed reaction wheels are named RWA 1, 2, and 3, respectively. In addition, Cassini has a backup, articulatable reaction wheel (RWA 4). Currently, RWA 3 is out of commission and the spin axis of RWA 4 is co-aligned with RWA 3. At Launch, RWA-4 was aligned parallel with RWA-1. On July 11, 2003, the platform was articulated to align the backup reaction wheel with the reaction wheel RWA-3, because the bearings of RWA-3 had developed occasional excessive frictional torque.[1,2,8] Each wheel has a wheel spin axis, with one direction designated as the positive spin direction. Location and orientation of Cassini reaction wheels are shown in Fig. 6.[1,2,11]

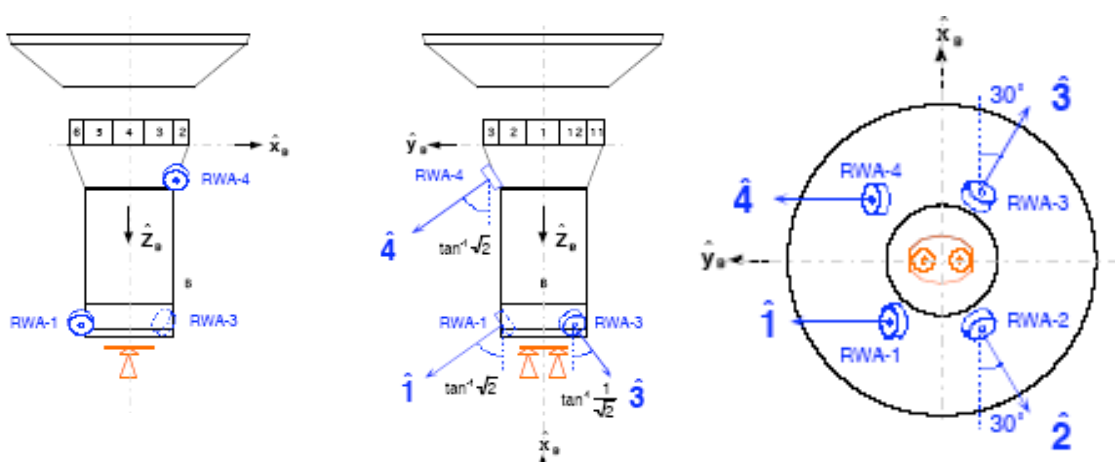

Fig. 6 Locations and orientation of Cassini reaction wheels.

The reaction wheel control system is a proportional-plus-derivative controller. This control system uses an algorithm that determines the desired torque on the spacecraft, and this torque vector is projected along each wheel axis to determine the contribution of each wheel.[11] The result is then negated to determine the commanded torque on each wheel. The torque of the wheel on the spacecraft is equal and opposite to the torque applied to the wheel itself.

The RWAs are used primarily for attitude control when precise and stable pointing of a science instrument is required during an observation. The advantages of using reaction wheels over thrusters are the conservation of hydrazine and the absence of unwanted ΔV imparted on the spacecraft.

The 3-axis angular momenta in RWA frame are transformed to the spacecraft's fixed frame via the transformation matrix given by Eq. 2. In this equation, the first two columns (for RWA-1 and 2) are determined pre-launch, and the last column (for RWA-4) is estimated after the RWA-4 articulation event in 2003.[1,2,8]

$$C_{RWA}^{SC} = \begin{bmatrix} 0 & -\frac{1}{\sqrt{2}} & 0.713318 \\ \sqrt{\frac{2}{3}} & -\frac{1}{\sqrt{6}} & -0.402252 \\ \frac{1}{\sqrt{3}} & \frac{1}{\sqrt{3}} & 0.573909 \end{bmatrix} \tag{2}$$

The RWA manager is an algorithm that accepts spacecraft torque requests from attitude control algorithms and attempts to satisfy those requests by commanding the appropriate wheel torques. It provides wheel momentum estimates to the attitude estimator algorithms and also is capable of enforcing speed control commands for each wheel used mainly to dump excess momentum that has accumulated in the wheels. The attitude control algorithm determines the desired torque on the spacecraft.[8,11] This torque vector is projected along each wheel axis to determine the contribution that each wheel is expected to contribute to the torque on the spacecraft. This value is then negated to determine the commanded torque on each wheel.[11] The torque of the wheel on the spacecraft is equal and opposite to the torque applied to the wheel itself. An imperfect motor receives this command and responds by putting out the motor torque. The motor torque must be summed with all other torques on the wheel to determine the accelerating or reaction torque. The friction and other torques either oppose or augment the motor torque depending on wheel speed and other effects.[11] The wheel accelerates under the influence of the reaction torque resulting in a particular wheel angle (and rate) time history. A digital tachometer counts the change in angle pulses and sends the results to the flight computer for further processing. The FSW filters the tachometer output to estimate the wheel speed. From the wheel speed and the estimated wheel inertia, the momentum parallel to the wheel axis can be computed. The momentum vectors from all the wheels are added to determine the total contribution of the reaction wheels to spacecraft momentum in spacecraft coordinates.[11] The data is then used by the attitude control algorithm in computing subsequent control torque commands.

The RWA hardware manager operates in three possible modes: the torque mode, the speed control mode, and the coast mode. The simplified block diagram of the speed control mode is depicted in Fig. 7.

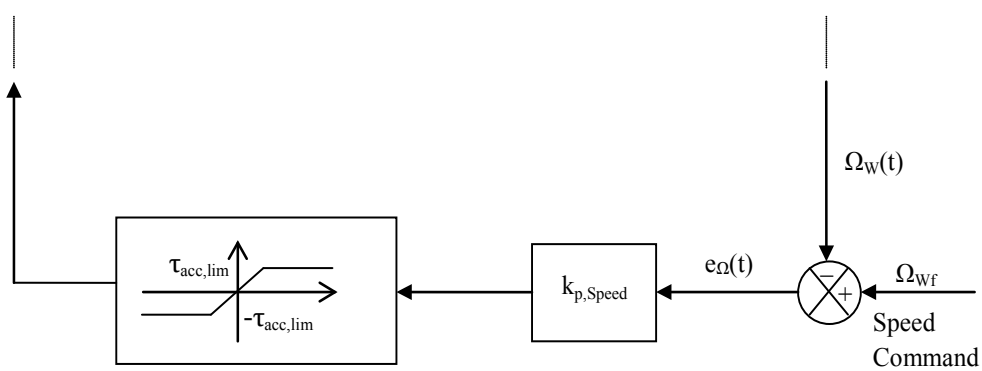

Fig. 7 The speed loop portion of the RWA hardware manager block diagram.

The error $e_\Omega(t)$ is the difference between the commanded RWA speed, which is the final RWA rate (Ω_{Wf}), and the ideal RWA speed, $\Omega_W(t)$. The function implemented by the RWA manager in speed control mode is individual wheel speed control. The simplified block diagram for the speed controller is shown in Fig. 7 for a single

wheel. As seen in Fig. 7, the speed command enters a summation block along with the ideal speed. The value of the accelerating torque limit, $\tau_{acc,lim}$, is set to 0.03 Nm as a default.[11]

The RWA angular rate and acceleration profiles can thus be determined, as shown in Fig.'s 8 and 9. The bias assumed in these two figures is changing the RWA-1 rate from 0 to +1000 RPM. The parameters t_0 and T are the start and end times of the bias for an RWA (RWa-1 in this case). The time t_1 marks the end of the linear range of the RWA rate profile. The rates Ω_W, Ω_{W0}, and Ω_{W1} are the RWA rate at times t, t_0, and t_1, respectively. The rate Ω_{Wf} is approximately the RWA rate at time T. When T is determined, we shall see that it is safe to assume that Ω_{Wf} is exactly the RWA rate at time T. The parameter $\dot{\Omega}_W$ is the RWA acceleration and τ_W is the time constant associated with the speed control loop. The *sgn(.)* is the signum (or "sign") function. The parameter τ_W equals:

$$\tau_W = \frac{1}{2\pi f_{n,SpeedLoop}} \tag{3}$$

The RWA angular acceleration and rate profiles for the ith RWA can be then reconstructed. The angular rate and acceleration profiles for one of the three RWAs (RWA-1) for a bias from 0 to +1000 RPM are shown if Fig.'s 8 and 9, respectively. Throughout the linear ramp region of the profiles, when $t_0 \le t \le t_1$:

$$\dot{\Omega}_W(t) = sgn(\Omega_{Wf} - \Omega_{W0})\frac{\tau_{acc,lim}}{I_{RWAi}} \tag{4}$$

$$\Omega_W(t) = \Omega_{W0} + sgn(\Omega_{Wf} - \Omega_{W0})\frac{\tau_{acc,lim}}{I_{RWAi}}(t - t_0) \tag{5}$$

Here, $\Omega_W(t_0) = \Omega_{W0}$ and $\Omega_W(T) \approx \Omega_{Wf}$, and I_{RWAi} is the moment of inertia of the ith RWA, with i = 1, 2, and 4 for the three prime RWAs. Once the RWA rate gets close the commanded rate, the speed control loop enters its linear range and the RWA rate and acceleration take the characteristic of exponentials.
Therefore, throughout the exponential region of the profiles, when $t_1 \le t \le T$:

$$\dot{\Omega}_W(t) = sgn(\Omega_{Wf} - \Omega_{W0})\frac{\tau_{acc,lim}}{I_{RWAi}} e^{\frac{-(t-t_1)}{\tau_W}} \tag{6}$$

$$\Omega_W(t) = \Omega_{W1} + sgn(\Omega_{Wf} - \Omega_{W0})\frac{\tau_{acc,lim}\tau_W}{I_{RWAi}}[1 - e^{\frac{-(t-t_1)}{\tau_W}}] \tag{7}$$

where once again i = 1, 2, and 4 for the three prime RWAs and $\Omega_W(t_1) = \Omega_{W1}$.
At the boundary of the linear range of speed control loop, i.e. at $t = t_1$, using Eq. 4:

$$t_1 = t_0 + sgn(\Omega_{Wf} - \Omega_{W0})\frac{I_{RWAi}}{\tau_{acc,lim}}(\Omega_{Wf} - \Omega_{W0}) - \tau_W \tag{8}$$

In order to determine the time T for the ith RWA, let $T = t_1 + n\tau_W$ and $N = \frac{\Omega_W(T) - \Omega_{W1}}{\Omega_{Wf} - \Omega_{W1}}$. Using Eq. 7 for T and the definition of N, we get $N = 1 - e^{-n}$ or $n = -ln(1 - N)$. The parameter N = 99.75% when n = 6, and this is the value we shall use for n. Therefore,

$$T = t_1 + 6\tau_W = t_0 + sgn(\Omega_{Wf} - \Omega_{W0})\frac{I_{RWAi}}{\tau_{acc,lim}}(\Omega_{Wf} - \Omega_{W0}) + 5\tau_W \tag{9}$$

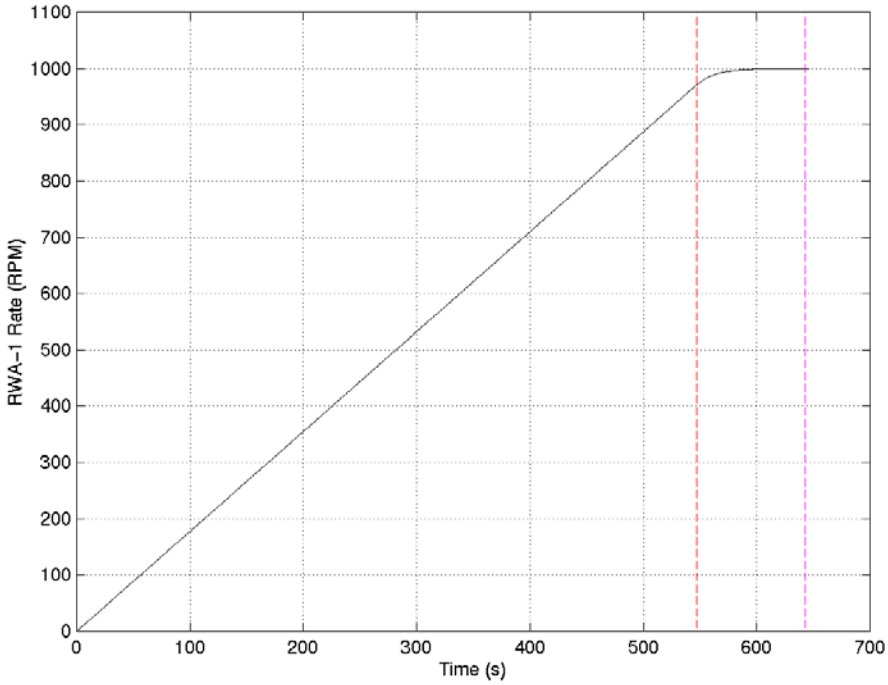

Fig. 8 RWA-1 angular rate profile for a bias event in which RWA-1 rate changes from 0 to +1000 RPM

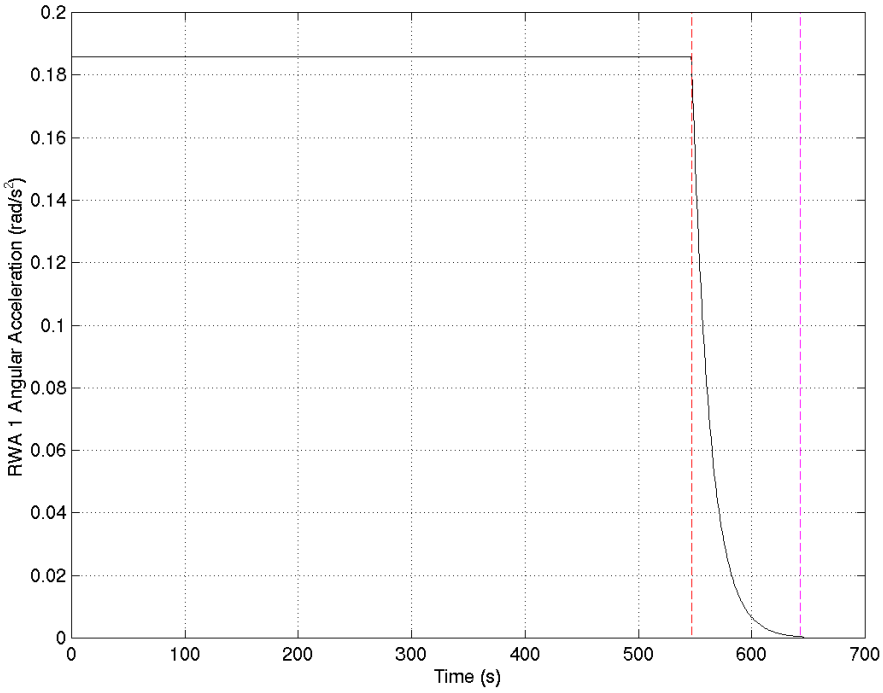

V. Thruster On-Time Determination for Ideal Thrusters

The RWA biases are always performed under RCS control and while the spacecraft is typically Earth-pointed with a good star coverage for star trackers, i.e. spacecraft's +X pointing along the Z-axis of the EME-2000 inertial frame. The attitude dead-band is typically 2 mrad along all three axes throughout the bias event. The Bang-off-Bang RCS controller maintains the spacecraft pointing while RWA rates change from their initial rates to their final commanded rates. The Euler equation of rotational dynamics for a spacecraft with reaction wheels is given by:

$$I\dot{\vec{\omega}} + \vec{\omega} \times (I\vec{\omega} + \vec{H}_{RWA}) = \vec{\tau}_{Dist} + \vec{\tau}_{Control} - \dot{\vec{H}}_{RWA} \tag{10}$$

where $\vec{\omega}$ is the spacecraft body rate in rad/s, $\vec{H}_{RWA}$ is the angular momentum of a set of three prime reaction wheels (RWA-1, RWA-2, and RWA-4) transformed to the spacecraft body frame in Nms, and $\vec{\tau}_{Control}$ and $\vec{\tau}_{Dist}$ are the control torque and disturbance torques in Nm, respectively. I is spacecraft's inertia tensor,[14]

$$I = \begin{pmatrix} I_{xx} & -I_{xy} & -I_{xz} \\ -I_{xy} & I_{yy} & -I_{yz} \\ -I_{xz} & -I_{yz} & I_{zz} \end{pmatrix}$$

Assuming the RCS control and negligible disturbance torques,

$$\frac{d}{dt}(I\vec{\omega} + \vec{H}_{RWA}) + \vec{\omega} \times (I\vec{\omega} + \vec{H}_{RWA}) = \vec{\tau}_{RCS} \tag{11}$$

where $\vec{\tau}_{RCS}$ is the torque generated by RCS thrusters. Integrating Eq. 11 and defining $S(\omega)$ as:

$$S(\vec{\omega}) = \begin{pmatrix} 0 & -\omega_z & \omega_y \\ \omega_z & 0 & -\omega_x \\ -\omega_y & \omega_x & 0 \end{pmatrix}$$

yields,

$$\int_{t_0}^{T} \frac{d}{dt}(I\vec{\omega} + \vec{H}_{RWA})dt + \int_{t_0}^{T} S(\vec{\omega})(I\vec{\omega} + \vec{H}_{RWA})dt = \int_{t_0}^{T} \vec{\tau}_{RCS} dt \tag{12}$$

The time t_0 is the start time of bias where all three RWAs are at their initial rates and time T is the end time of the bias where all RWAs have reached their final (commanded) rates. Also,

$$\int_{t_0}^{T} \vec{\tau}_{RCS} dt = \sum_i \vec{L}_{arm,i} \times \vec{F}_{thr,i}[T_{on,i}(T) - T_{on,i}(t_0) + \frac{I_{res,i}}{|\vec{F}_{thr,i}|}] \tag{13}$$

where, i = 1, …, 8 for the eight RCS primary branch thrusters, i.e. $i \in \{Z_1, Z_2, Z_3, Z_4, Y_1, Y_2, Y_3, Y_4\}$. The parameter $T_{on,i}$ is the ith thruster's on-time in seconds, $\vec{L}_{arm,i}$ and $\vec{F}_{thr,i}$ are the moment arm vector for the ith thruster and its thrust vector, respectively. In order to computer $\vec{L}_{arm,i}$ the vector associated with the center of mass (c.m.) location[13] must be subtracted from the thruster locations. The parameter $I_{res,i}$ is the residual impulse of the ith thruster. The residual impulse for a single thruster pulse of width Δ equals is given by Eq. 1.

Since throughout the RWA bias event, the spacecraft is Earth-pointed and not slewing, it is safe to assume that spacecraft body rate is negligible throughout the bias event. Therefore,

$$I[\cancelto{\approx 0}{\vec{\omega}(T) - \vec{\omega}(t_0)}] + [\vec{H}_{RWA}(T) - \vec{H}_{RWA}(t_0)] + I\cancelto{\approx 0}{\int_{t_0}^{T} S(\vec{\omega})\vec{\omega}dt} + \cancelto{\approx 0}{\int_{t_0}^{T} S(\vec{\omega})\vec{H}_{RWA}dt} = \int_{t_0}^{T} \vec{\tau}_{RCS} dt \tag{14}$$

As we shall see later, we have to account for the cancelled terms in the above equation when we determine the flight calibrated thruster on-times. Therefore, we can write:

$$\Delta\vec{H} = \vec{H}_{RWA}(T) - \vec{H}_{RWA}(t_0) = \sum_i \vec{L}_{arm,i} \times \vec{F}_{thr,i}[T_{on,i}(T) - T_{on,i}(t_0) + (t_T - t_R)] \tag{15}$$

across the RWA bias event, i.e. from t_0 to T. The term $\Delta\vec{H}$ equals:

$$\Delta\vec{H} = C_{RWA}^{SC} diag(I_{RWA1}, I_{RWA2}, I_{RWA4})\Delta\vec{\Omega}_{RWA} \tag{16}$$

where

$$\Delta\vec{\Omega}_{RWA} = \vec{\Omega}_{RWA,f} - \vec{\Omega}_{RWA,i} \tag{17}$$

Here, C_{RWA}^{SC} is the transformation matrix from RWA frame to spacecraft body frame, given by Eq. 2, and *diag(a,b,c)* is a 3×3 diagonal matrix with *a*, *b*, and *c* along the main diagonal.

Fig. 10 depicts the three components of $\Delta\vec{H}$ vector output from the ground software (GSW) tool, side by side with the FSDS simulation output for the RWA bias event that occurred on February 13, 2010 in which $\vec{\Omega}_{RWA,i}$ = [+1078, +1146, +1047]^T RPM and $\vec{\Omega}_{RWA,f}$ = [+432, -1293, -508]^T RPM. As seen in this figure, the GSW output matches closely with the FSDS output.

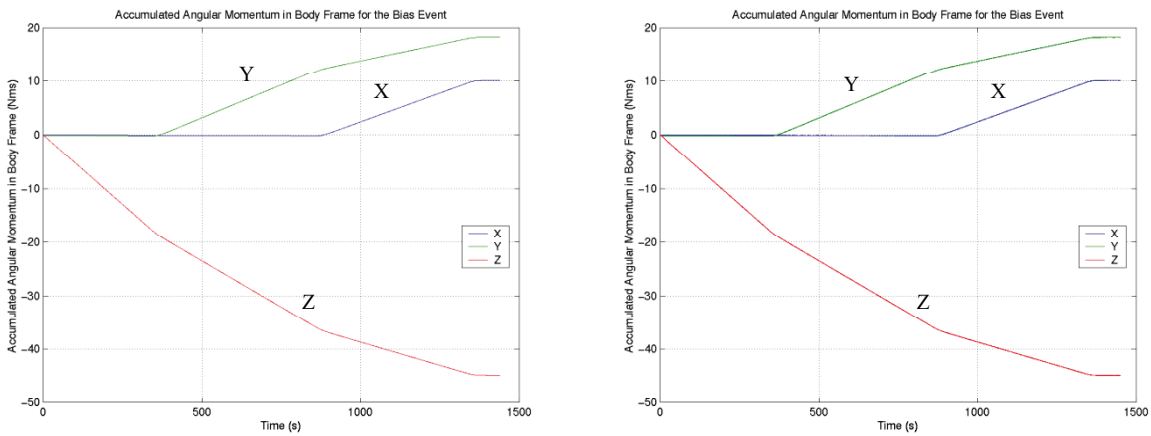

(a) GSW output **(b) FSDS output**

Fig. 10 The angular momentum profile in spacecraft body frame, $\Delta\vec{H}$, for 2/13/2010 bias.

Fig. 11 depicts the steps involved in the methodology described in this paper. Various algorithms of this methodology are implemented in the GSW tool developed by the author. There are four blocks in Fig. 11 with the block titled "Ideal RCS On-time Determination" being the core block. The inputs consist of the array of thruster magnitudes for eight primary RCS thrusters, $F_{thr,array}$, the spacecraft wet mass, M_{sc}, the spacecraft c.m. location in spacecraft coordinate frame, $C\vec{M}$, and the initial and final RWA rates, $\vec{\Omega}_{RWA,i}$ and $\vec{\Omega}_{RWA,f}$. All the programmable and constant parameters used in the entire GSW are set in the block titled "Parameter Set-up."

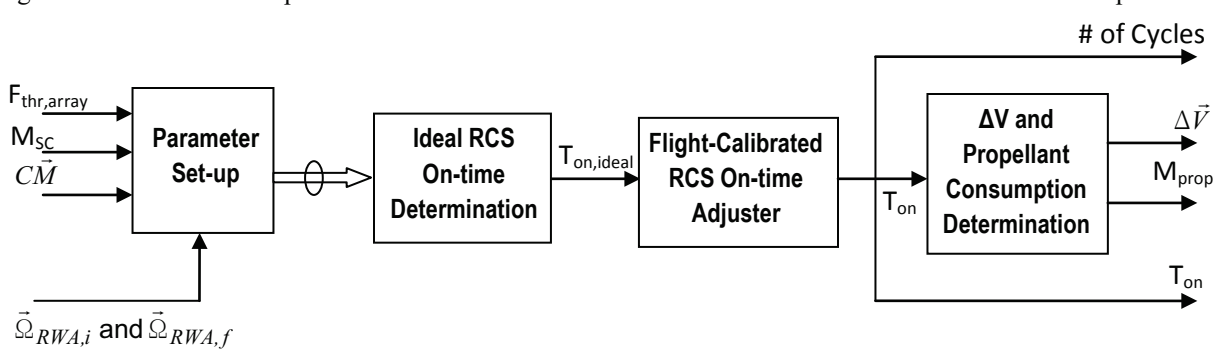

Fig. 11 Block diagram of the methodology for determining thruster on-times, ΔV, and consumed propellant.

After setting up the initial parameters, the GSW computes the angular momentum profile due to RWA rate changes in body frame, $\Delta\vec{H}$ inside the Ideal RCS On-time Determination block. In order to determine this angular momentum, first a set of three time tags for each RWA is determined which includes the time tag for the start of each RWA rate change, $t_{0,RWAi}$, the end time for the linear range of RWA rate change, $t_{1,RWAi}$, and the time tag for the end time of the bias for each RWA, T_{RWAi} with i = 1, 2, and 4. The difference between the maximum of the three T_{RWAi} times and the minimum of the three $t_{0,RWAi}$ times is the bias time duration, T_{max}. Therefore,

$$T_{max} = max\{T_{RWA1}, T_{RWA2}, T_{RWA4}\} - min\{t_{0,RWA1}, t_{0,RWA2}, t_{0,RWA4}\} \quad (18)$$

The GSW runs at every s_{sample} sample period, where s_{sample} is reprogrammable and is typically equal to 1 s. At every sample period, the vector $\Delta\vec{H}$ is input to a module within the Ideal RCS On-time Determination block that computes the RCS on-times during the sample period assuming ideal, rectangular thruster pulses, i.e. the residual impulse effect is ignored. This means that the on-times are determined theoretically. There are altogether 10 different cases and the GSW determines which case applies during each sample period. The derivations of subsequent equations are not given in this paper. Additionally, the total ΔV and the total consumed propellant, M_{prop}, are computed in the last block of Fig. 11 using the flight-calibrated total thruster on-times. In current Cassini spacecraft condition and in general for post Probe release scenarios, $CM_x > 0$, $CM_y > 0$, and $CM_z > 0$, where CM_x, CM_y, and CM_z are the three components of spacecraft's c.m. in body coordinates, $\vec{CM}$.[13]

The specific impulse of an RCS thruster is a nonlinear function of the thruster firing average duty cycle (μ). For RWA bias events, the maximum average duty cycles, $\mu_{max,bias}$, are no more than a few percent. Using Cassini flight data, an empirical formula was developed by this author, subsequently modified by Emily B. Pilinski, a former AACS team member, and further tweaked by this author to determine each thruster's specific impulse given its average duty cycle. Eq. 19 below captures this empirical formula:

$$I_{sp}(\mu) = P_0 - P_1 e^{-P_2\mu} - P_3 e^{-P_4\mu} \quad \text{[s]} \quad (\text{for } 0 \le \mu \le \mu_{max,bias}) \quad (19)$$

The coefficients in this equation are given by: $\vec{P} = [P_0, P_1, P_2, P_3, P_4]$.

Theoretical Thruster On-Time Determination Algorithm

Only one representative case is mentioned here out of a total of 10 different cases that arise inside the algorithm.

Representative Case: $\Delta\vec{H} = [\Delta H_x, \Delta H_y, 0]^T$ with $\Delta H_x > 0$ and $\Delta H_y > 0$. Thrusters: (Z_1, Z_4) or (Z_3, Z_4) with Z_4 exercised the most.

The diagram in Fig. 12 should clarify the geometric set-up. Similar diagrams could be made to clarify the other cases. The three angles θ_{Z1}, θ_{Z3}, and θ_{Z4} made between the torque vectors associated with firing Z_1, Z_3, and Z_4 thrusters are defined in Fig. 12.

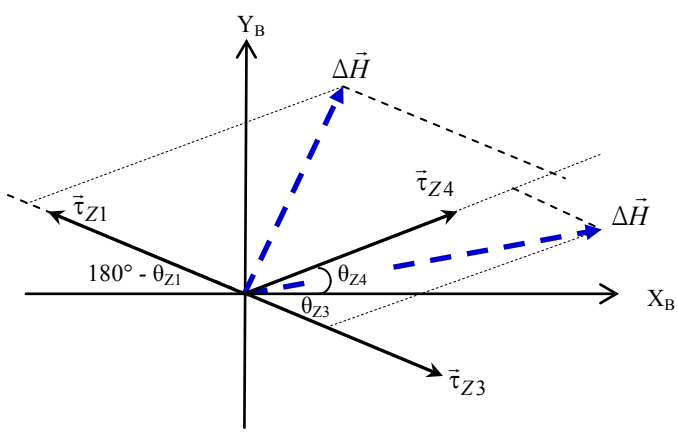

$$\theta_{Z1} = 180° + Tan^{-1}\left(-\frac{L_x - CM_x}{L_y - CM_y}\right)$$

$$\theta_{Z3} = Tan^{-1}\left(-\frac{L_x + CM_x}{L_y + CM_y}\right)$$

$$\theta_{Z4} = Tan^{-1}\left(\frac{L_x - CM_x}{L_y + CM_y}\right)$$

Fig. 12 A vector diagram for the representative case with angles θ_{Z1}, θ_{Z3}, θ_{Z4} defined.

If $\frac{\Delta H_y}{\Delta H_x} = \frac{L_x - CM_x}{L_y + CM_y}$, then $T_{on,Z_1} = T_{on,Z_3} = 0$. If $0 < \frac{\Delta H_y}{\Delta H_x} < \frac{L_x - CM_x}{L_y + CM_y}$, the on-time of Z_3 and Z_4 thrusters, and if $\frac{\Delta H_y}{\Delta H_x} > \frac{L_x - CM_x}{L_y + CM_y}$, the on-times of Z_1 and Z_4 thrusters are computed analytically.

VI. Flight-Calibrated Thruster On-Times

Fig. 13.a below depicts per-axis attitude control error from the FSDS simulation of the RWA bias event on February 13, 2010. The commanded dead-band was the usual [2, 2, 2] mrad. As seen in this figure, the thruster firings cause the attitude control errors to move to one side of the dead-band. The excursions due to the walking dead-band are also seen in Fig. 14.a. Thruster pulses for a typical RWA bias event are usually 125 ms wide, but also consecutive 125 ms firings construct pulses that are 250 ms wide.

As stated earlier, the RCS controller algorithms are designed to use the error signals, which are the weighted sums of attitude and rate errors, to control thruster firings in the presence of the commanded attitude dead-band. If these errors are not sufficiently large, no thruster firing is requested and as a result, the angular momentum profile from thruster firings stay entirely above or below $\Delta\vec{H}$, the angular momentum of the RWAs transformed to the body frame (see Fig.'s 14.a and 16.a below). On the other hand, when these errors are sufficiently large, the angular momentum profile from thruster firings overshoots the $\Delta\vec{H}$ profile (see Fig.'s 13.b and 15.a). The reconstructed angular momentum in the spacecraft body frame using RCS thruster firings is coarse (see Fig. 13.b and compare it with Fig. 10.b) and does not quite track $\Delta\vec{H}$ profile. The difference of the two profiles is captured in Fig.'s 14.b, 15.b, and 16.b for each of the three axes.

The bottom line is that because of the RCS controller's characteristics, per-axis angular momentum profile from thruster firings deviates from the respective angular momentum profile from the RWA spin rate changes in spacecraft body frame, and at the end of the bias event, the difference of the two per-axis profiles is a few Nms. After examination of these difference profiles from FSDS simulations and flight data of several bias events, these differences are modeled to adjust the RCS thruster on-times. The flight-calibrated thruster on-time adjustments are summarized in steps given below.

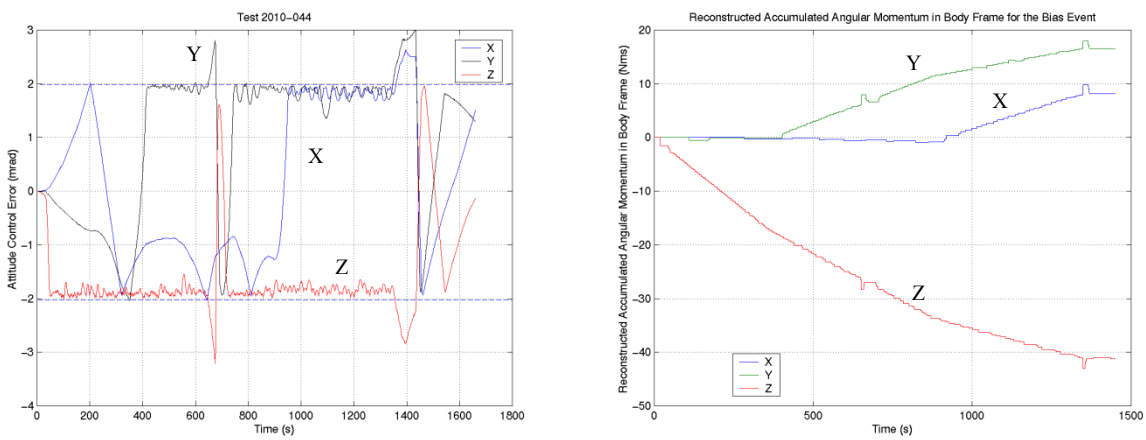

(a) **(b)**

Fig. 13 (a) The attitude control error from FSDS simulation of the bias on 2/13/2010. (b) The reconstructed angular momentum in spacecraft body frame using thruster on-times from FSDS simulation.

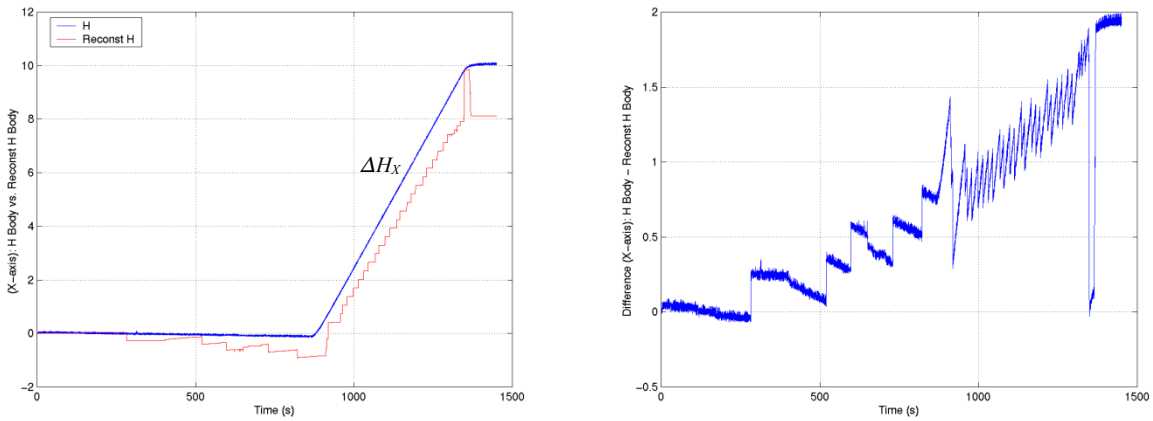

(a) **(b)**

Fig. 14 (a) The X-axis angular momentum from RWAs in body frame superimposed on the reconstructed X-axis angular momentum in body frame using thruster on-times from FSDS simulation of the bias on 2/13/2010. (b) The difference of the two profiles.

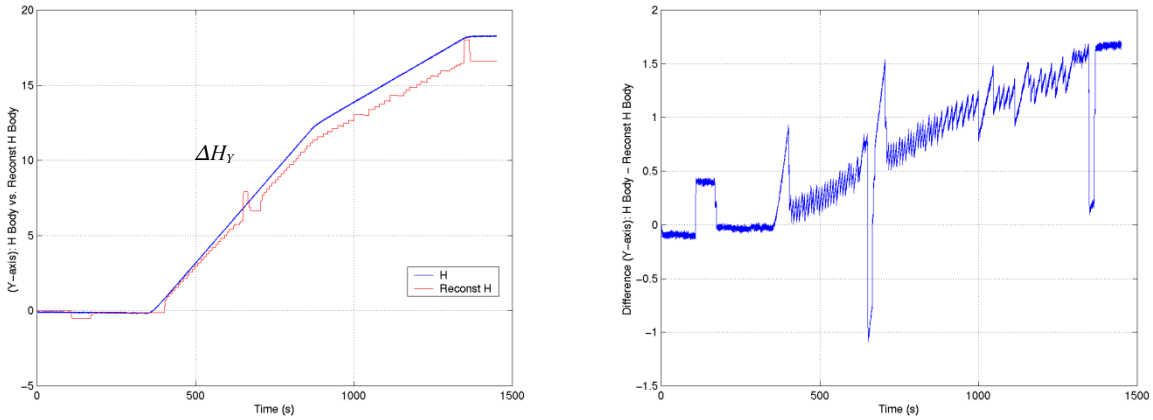

(a) **(b)**

Fig. 15 (a) The Y-axis angular momentum from RWAs in body frame superimposed on the reconstructed Y-axis angular momentum in body frame using thruster on-times from FSDS simulation of the bias on 2/13/2010. (b) The difference of the two profiles.

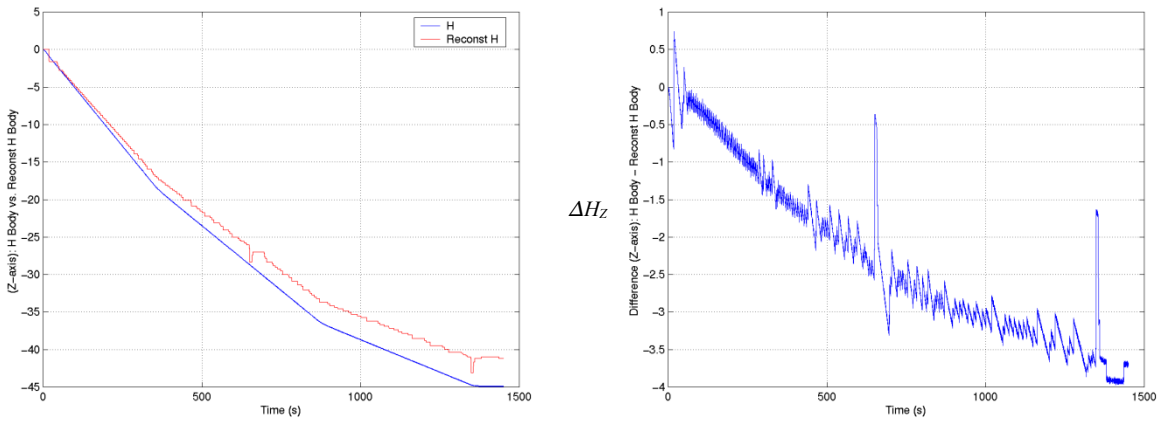

(a) **(b)**

Fig. 16 (a) The Z-axis angular momentum from RWAs in body frame superimposed on the reconstructed Z-axis angular momentum in body frame using thruster on-times from FSDS simulation of the bias on 2/13/2010. (b) The difference of the two profiles.

Inside the "Parameter Set-up" block of Fig. 11, a gain array is initialized. The entries of this gain array are used for thruster on-time adjustments. To account for the effect of the residual impulse due to the rise and tail-off time constants of thruster pulses, each ideal thruster on-time, $T_{on,i,ideal}$, is adjusted. The thruster on-times of Y-facing thrusters, i.e. Y_1, Y_2, Y_3, and Y_4, are subsequently adjusted to account for the modeled Z-axis angular momentum deviations (see Fig. 16).

The thruster on-times of Z-facing thrusters, i.e. Z_1, Z_2, Z_3, and Z_4, are also adjusted by a term. A Boolean flag indicting that the bias is done mainly with Y-facing thrusters, is set to TRUE, when the bias is done mainly with Y-facing thrusters. In this case, the Z-facing thruster on-times are small but not zero, and hence, greater adjustments are required. If this Boolean flag is FALSE, the angular momentum in body frame at the end of the bias event is first determined and set equal to $\vec{h}$:

$$\vec{h} = [h_x, h_y, h_z]^T = \Delta\vec{H}(T_{max}) \tag{20}$$

Then, the on-time of Z-facing thrusters are adjusted, using a set of matrix equation, depending on whether $sgn(h_x)\cdot sgn(h_y)$ = -1, +1, or 0. The number of thruster cycles for each RCS thruster, $N_{cyc,i}$, is also determined from thruster on-times. The parameter $N_{cyc,i}$ is then rounded to become a non-negative integer.

VII. ΔV and Propellant Consumption Determination

The total mass of hydrazine used up for the bias event is determined by:

$$M_{prop} = \frac{1}{g_0}\sum_i \frac{F_{thr,i}T_{on,i}}{I_{sp,i}} \text{ [kg]} \tag{21}$$

where, i = 1, …, 8 for the eight RCS primary branch thrusters, i.e. $i \in \{Z_1, Z_2, Z_3, Z_4, Y_1, Y_2, Y_3, Y_4\}$.
The parameter g_0 = 9.8065 m/s^2 is the Earth's gravitational acceleration at the sea level. $I_{sp,i}$ is determined for the ith thruster using the total thruster on-time for the ith thruster, $T_{on,i}$, T_{max} defined by Eq. 18, and the empirical formula given by Eq. 19. The ΔV vector in spacecraft body frame is determined by:

$$\Delta\vec{V}^{Body} = \frac{1}{M_{SC}}\sum_j \vec{F}_{thr,j}T_{on,j} \text{ [m/s]} \tag{22}$$

where, j = 1, …, 4 for the eight RCS primary branch thrusters, i.e. $j \in \{Z_1, Z_2, Z_3\}$, and M_{SC} is the spacecraft's wet mass in kg. Since throughout the RWA bias, the spacecraft's attitude is almost fixed in inertial frame, the $\Delta\vec{V}^{Body}$ can be transformed to the EME-2000 frame using the transformation matrix from spacecraft body frame to EME-2000 inertial frame ($C_{Body}^{EME2000}$).

$$\Delta\vec{V}^{EME2000} = C_{Body}^{EME2000} \cdot \Delta\vec{V}^{Body} \quad \text{[m/s]} \tag{23}$$

The transformation matrix $C_{Body}^{EME2000}$ is determined from the inertial-to-body quaternion. The ΔV's are often presented in mm/s.

VIII. Comparing Results for Eight Reaction Wheel Bias Events

The methodology and the algorithms used in the GSW are validated using both FSDS simulation and flight data. Multiple FSDS simulations are run and the flight data from a dozen of RWA biases are examined. Tables 3.a through 3.h below compare the GSW outputs against both the FSDS simulation outputs and flight data for eight RWA bias events. As seen, in these tables, in general, FSDS generated thruster on-times and pulses tend to be higher than the respective flight data. Also, it can be observed the flight-calibrated on-times are closer to both FSDS and flight compared to the theoretical, unadjusted on-times. Also, it is observed that when averaged over the eight bias cases, the average difference of on-times between the flight data and GSW is ~0.59 s, the average difference in Z-axis ΔV is ~0.79 mm/s, and the average difference in hydrazine mass is ~1.05 grams.

Table 3.a Comparing Results for RWA Bias Event on August 22, 2009

RWA Bias Event: 08/22/2009 (DOY 234) Thrust = 0.77 N		GSW[1] (Ideal)	GSW[2]	FSDS Simulation	Flight Data	Abs. Diff. Flight – GSW	%Abs. Diff.[3] (per Flight)
Initial RWA Rates	*RPM*	[-1118, +1290, +330] *(for RWA-1, 2, 4)*				-	-
Final RWA Rates	*RPM*	[+626, +1300, -729] *(for RWA-1, 2, 4)*				-	-
Bias Size (RWA Rate Change)	*RPM*	[+1744, +10, -1059]				-	-
Bias Time Duration	*s*	1062				-	-
ΔT_{on} Y_1-Y_3 Thruster Pair	*s*	0.00	0.00	0.75	0.25	0.25	100
ΔT_{on} Y_2-Y_4 Thruster Pair	*s*	3.62	3.53	4.25	3.62	0.09	2
ΔT_{on} Z_1 Thruster	*s*	23.96	24.39	24.78	23.43	0.96	4
ΔT_{on} Z_2 Thruster	*s*	0.00	6.36	6.63	5.99	0.37	6
ΔT_{on} Z_3 Thruster	*s*	0.00	2.12	1.13	1.25	0.87	70
ΔT_{on} Z_4 Thruster	*s*	12.52	17.99	18.28	17.69	0.30	2
Total Z-Facing RCS ΔT_{on}	*s*	36.47	50.86	50.81	48.36	2.50	5
# of Y_1-Y_3 Firing Cycles	-	-	0	6	2	2	100
# of Y_2-Y_4 Firing Cycles	-	-	23	26	28	5	19
# of Z_1 Firing Cycles	-	-	156	179	180	24	13
# of Z_2 Firing Cycles	-	-	41	48	48	7	15
# of Z_3 Firing Cycles	-	-	14	6	9	5	51
# of Z_4 Firing Cycles	-	-	115	137	141	26	18
ΔV_x in Body Frame	*mm/s*	0.00	0.00	0.04	0.03	0.03	100
ΔV_y in Body Frame	*mm/s*	0.00	0.00	0.03	0.02	0.02	100
ΔV_z in Body Frame	*mm/s*	-11.63	-16.22	-17.49	-16.60	0.38	2
ΔV (Magnitude)	*mm/s*	11.63	16.22	17.49	16.60	0.38	2
Consumed Hydrazine Mass	*grams*	21.4	28.4	26.6	27.0	1.4	5

[1] Assumes rectangular thruster pulses and is not flight-calibrated.

[2] Flight-calibrated ground software outputs with modeled thruster pulses incorporated (using rise time and tail off time constants).

[3] The percent difference between the flight data and the GSW outputs relative to the flight data.

Table 3.b Comparing Results for RWA Bias Event on October 5, 2009

RWA Bias Event: 10/05/2009 (DOY 278) Thrust = 0.77 N		GSW (Ideal)	GSW	FSDS Simulation	Flight Data	Abs. Diff. Flight – GSW	%Abs. Diff. (per Flight)
Initial RWA Rates	*RPM*	[-1026, -752, -322]				-	-
Final RWA Rates	*RPM*	[+1124, -1278, +359]				-	-
Bias Size (RWA Rate Change)	*RPM*	[+2150, -526, +681]				-	-
Bias Time Duration	*s*	1291				-	-
ΔT_{on} Y_1-Y_3 Thruster Pair	*s*	0.00	0.00	0.75	0.86	0.86	100
ΔT_{on} Y_2-Y_4 Thruster Pair	*s*	11.84	11.55	11.96	11.82	0.26	2
ΔT_{on} Z_1 Thruster	*s*	12.17	17.41	17.89	17.06	0.35	2
ΔT_{on} Z_2 Thruster	*s*	0	2.03	2.38	1.31	0.72	55
ΔT_{on} Z_3 Thruster	*s*	0.67	6.27	5.84	6.25	0.02	0
ΔT_{on} Z_4 Thruster	*s*	22.17	22.65	22.83	22.12	0.52	2

Total Z-Facing RCS ΔT_{on}	*s*	35.01	48.36	48.93	46.74	1.62	3
# of Y_1-Y_3 Firing Cycles	-	-	0	3	6	6	100
# of Y_2-Y_4 Firing Cycles	-	-	74	87	90	16	18
# of Z_1 Firing Cycles	-	-	111	130	131	20	15
# of Z_2 Firing Cycles	-	-	13	14	8	5	63
# of Z_3 Firing Cycles	-	-	40	41	45	5	11
# of Z_4 Firing Cycles	-	-	145	156	168	23	14
ΔV_x in Body Frame	*mm/s*	0.00	0.00	0.04	0.02	0.02	100
ΔV_y in Body Frame	*mm/s*	0.00	0.00	-0.01	0.00	0.00	100
ΔV_z in Body Frame	*mm/s*	-11.19	-15.60	-16.82	-16.19	0.60	4
ΔV (Magnitude)	*mm/s*	11.19	15.60	16.82	16.19	0.60	4
Consumed Hydrazine Mass	*grams*	29.0	35.5	32.5	33.0	2.5	8

Table 3.c Comparing Results for RWA Bias Event on December 13, 2009

RWA Bias Event: 12/13/2009 (DOY 347) Thrust = 0.76 N	**GSW (Ideal)**	**GSW**	**FSDS Simulation**	**Flight Data**	**Abs. Diff. Flight – GSW**	**%Abs. Diff. (per Flight)**
Initial RWA Rates	*RPM*	[-482, +1233, +965]			-	-
Final RWA Rates	*RPM*	[-959, +1296, +324]			-	-
Bias Size (RWA Rate Change)	*RPM*	[-477, +63, -641]			-	-
Bias Time Duration	*s*	445			-	-
ΔT_{on} Y_1-Y_3 Thruster Pair	*s*	5.46	5.33	5.13	5.31	0.02	0
ΔT_{on} Y_2-Y_4 Thruster Pair	*s*	0.00	0.00	0.00	0.25	0.25	100
ΔT_{on} Z_1 Thruster	*s*	2.56	3.63	4.25	4.12	0.49	12
ΔT_{on} Z_2 Thruster	*s*	4.60	4.69	4.88	4.87	0.18	4
ΔT_{on} Z_3 Thruster	*s*	0.03	1.28	1.38	1.62	0.34	21
ΔT_{on} Z_4 Thruster	*s*	0.00	0.42	0.75	0.87	0.45	52
Total Z-Facing RCS ΔT_{on}	*s*	7.18	10.01	11.25	11.48	1.47	13
# of Y_1-Y_3 Firing Cycles	-	-	34	29	40	6	15
# of Y_2-Y_4 Firing Cycles	-	-	0	0	2	2	100
# of Z_1 Firing Cycles	-	-	23	29	33	10	30
# of Z_2 Firing Cycles	-	-	30	42	39	9	23
# of Z_3 Firing Cycles	-	-	8	18	13	5	37
# of Z_4 Firing Cycles	-	-	3	5	7	4	62
ΔV_x in Body Frame	*mm/s*	0.00	0.00	0.00	0.00	0.00	100
ΔV_y in Body Frame	*mm/s*	0.00	0.00	0.01	0.01	0.01	100
ΔV_z in Body Frame	*mm/s*	-2.27	-3.17	-3.88	-3.85	0.68	18
ΔV (Magnitude)	*mm/s*	2.27	3.17	3.88	3.85	0.68	18
Consumed Hydrazine Mass	*grams*	8.9	10.1	9.4	10.0	0.1	1

Table 3.d Comparing Results for RWA Bias Event on February 13, 2010

RWA Bias Event: 02/13/2010 (DOY 044) Thrust = 0.75 N	**GSW (Ideal)**	**GSW**	**FSDS Simulation**	**Flight Data**	**Abs. Diff. Flight – GSW**	**%Abs. Diff. (per Flight)**
Initial RWA Rates	*RPM*	[+1078, +1146, +1047]			-	-
Final RWA Rates	*RPM*	[+432, -1293, -508]			-	-
Bias Size (RWA Rate Change)	*RPM*	[-646, -2439, -1555]			-	-
Bias Time Duration	*s*	1440			-	-
ΔT_{on} Y_1-Y_3 Thruster Pair	*s*	24.25	23.67	24.14	23.64	0.03	0
ΔT_{on} Y_2-Y_4 Thruster Pair	*s*	0.00	0.00	1.88	1.38	1.38	100
ΔT_{on} Z_1 Thruster	*s*	7.77	11.29	12.94	12.52	1.24	10
ΔT_{on} Z_2 Thruster	*s*	0.07	1.42	2.88	2.50	1.08	43
ΔT_{on} Z_3 Thruster	*s*	0.50	4.53	4.87	5.12	0.59	12
ΔT_{on} Z_4 Thruster	*s*	15.00	15.30	16.59	16.39	1.10	7
Total Z-Facing RCS ΔT_{on}	*s*	23.33	32.53	37.28	36.53	4.00	11
# of Y_1-Y_3 Firing Cycles	-	-	151	160	182	31	17
# of Y_2-Y_4 Firing Cycles	-	-	0	6	7	7	100
# of Z_1 Firing Cycles	-	-	72	91	96	24	25
# of Z_2 Firing Cycles	-	-	9	13	19	10	52
# of Z_3 Firing Cycles	-	-	29	33	42	13	31

# of Z_4 Firing Cycles	-	-	98	113	121	23	19
ΔV_x in Body Frame	*mm/s*	0.00	0.00	0.02	0.02	0.02	100
ΔV_y in Body Frame	*mm/s*	0.00	0.00	-0.02	0.01	0.01	100
ΔV_z in Body Frame	*mm/s*	-7.35	-10.25	-12.61	-12.36	2.10	17
ΔV (Magnitude)	*mm/s*	7.35	10.25	12.61	12.36	2.10	17
Consumed Hydrazine Mass	*grams*	34.4	38.3	38.8	39.0	0.7	2

Table 3.e Comparing Results for RWA Bias Event on March 3, 2010

RWA Bias Event: 03/03/2010 (DOY 062) Thrust = 0.75 N		**GSW (Ideal)**	**GSW**	**FSDS Simulation**	**Flight Data**	**Abs. Diff. Flight – GSW**	**%Abs. Diff. (per Flight)**
Initial RWA Rates	*RPM*	[-1094, -731, -909]				-	-
Final RWA Rates	*RPM*	[-1355, -744, -642]				-	-
Bias Size (RWA Rate Change)	*RPM*	[-261, -13, +267]				-	-
Bias Time Duration	*s*	234				-	-
ΔT_{on} Y_1-Y_3 Thruster Pair	*s*	0.13	0.12	0.13	0.63	0.50	80
ΔT_{on} Y_2-Y_4 Thruster Pair	*s*	0.07	0.07	0.13	0.50	0.43	87
ΔT_{on} Z_1 Thruster	*s*	0.00	0.30	0.00	0.38	0.08	21
ΔT_{on} Z_2 Thruster	*s*	1.24	2.05	2.50	2.63	0.58	22
ΔT_{on} Z_3 Thruster	*s*	3.93	3.95	3.63	3.75	0.20	5
ΔT_{on} Z_4 Thruster	*s*	0.00	0.90	1.13	1.50	0.60	40
Total Z-Facing RCS ΔT_{on}	*s*	5.16	7.20	7.25	8.26	1.06	13
# of Y_1-Y_3 Firing Cycles	-	-	1	1	5	4	84
# of Y_2-Y_4 Firing Cycles	-	-	0	1	4	4	89
# of Z_1 Firing Cycles	-	-	2	0	3	1	36
# of Z_2 Firing Cycles	-	-	13	11	21	8	38
# of Z_3 Firing Cycles	-	-	25	19	30	5	16
# of Z_4 Firing Cycles	-	-	6	8	12	6	52
ΔV_x in Body Frame	*mm/s*	0.00	0.00	0.00	-0.01	0.01	100
ΔV_y in Body Frame	*mm/s*	0.00	0.00	-0.01	-0.01	0.01	100
ΔV_z in Body Frame	*mm/s*	-1.63	-2.27	-2.42	-2.73	0.46	17
ΔV (Magnitude)	*mm/s*	1.63	2.27	2.42	2.73	0.46	17
Consumed Hydrazine Mass	*grams*	2.7	3.7	3.3	4.0	0.3	9

Table 3.f Comparing Results for RWA Bias Event on March 19, 2010

RWA Bias Event: 03/19/2010 (DOY 078) Thrust = 0.75 N		**GSW (Ideal)**	**GSW**	**FSDS Simulation**	**Flight Data**	**Abs. Diff. Flight – GSW**	**%Abs. Diff. (per Flight)**
Initial RWA Rates	*RPM*	[-928, -744, -435]				-	-
Final RWA Rates	*RPM*	[+844, -844, -919]				-	-
Bias Size (RWA Rate Change)	*RPM*	[+1772, -100, -484]				-	-
Bias Time Duration	*s*	1078				-	-
ΔT_{on} Y_1-Y_3 Thruster Pair	*s*	0.49	0.48	1.40	1.13	0.64	57
ΔT_{on} Y_2-Y_4 Thruster Pair	*s*	6.77	6.61	7.43	7.08	0.47	7
ΔT_{on} Z_1 Thruster	*s*	19.53	20.14	21.11	18.94	1.20	6
ΔT_{on} Z_2 Thruster	*s*	0.00	5.96	4.69	3.63	2.33	64
ΔT_{on} Z_3 Thruster	*s*	0.00	1.99	1.75	1.50	0.49	33
ΔT_{on} Z_4 Thruster	*s*	14.69	19.62	18.17	16.81	2.81	17
Total Z-Facing RCS ΔT_{on}	*s*	34.22	47.71	45.72	40.88	6.83	17
# of Y_1-Y_3 Firing Cycles	-	-	3	6	8	5	61
# of Y_2-Y_4 Firing Cycles	-	-	42	46	53	11	20
# of Z_1 Firing Cycles	-	-	129	150	144	15	10
# of Z_2 Firing Cycles	-	-	38	32	25	13	53
# of Z_3 Firing Cycles	-	-	13	9	9	4	41
# of Z_4 Firing Cycles	-	-	126	127	127	1	1
ΔV_x in Body Frame	*mm/s*	0.00	0.00	0.03	0.04	0.04	100
ΔV_y in Body Frame	*mm/s*	0.00	0.00	0.03	0.01	0.01	100
ΔV_z in Body Frame	*mm/s*	-10.79	-15.04	-15.51	-13.86	1.18	9
ΔV (Magnitude)	*mm/s*	10.79	15.04	15.51	13.86	1.18	9
Consumed Hydrazine Mass	*grams*	23.4	29.7	27.6	28.0	1.7	6

Table 3.g Comparing Results for RWA Bias Event on March 24, 2010

RWA Bias Event: 03/24/2010 (DOY 083) Thrust = 0.75 N		GSW (Ideal)	GSW	FSDS Simulation	Flight Data	Abs. Diff. Flight – GSW	%Abs. Diff. (per Flight)
Initial RWA Rates	*RPM*	[-667, -660, -1263]				-	-
Final RWA Rates	*RPM*	[-860, -867, -305]				-	-
Bias Size (RWA Rate Change)	*RPM*	[-193, -207, +958]				-	-
Bias Time Duration	*s*	624				-	-
ΔT_{on} Y_1-Y_3 Thruster Pair	*s*	0.96	0.94	1.60	1.12	0.17	16
ΔT_{on} Y_2-Y_4 Thruster Pair	*s*	3.90	3.80	4.50	3.91	0.11	3
ΔT_{on} Z_1 Thruster	*s*	0.00	0.66	1.25	0.18	0.48	-
ΔT_{on} Z_2 Thruster	*s*	0.01	1.98	3.54	3.18	1.20	38
ΔT_{on} Z_3 Thruster	*s*	9.23	9.24	9.19	8.25	0.99	12
ΔT_{on} Z_4 Thruster	*s*	2.05	3.87	5.43	5.24	1.37	26
Total Z-Facing RCS ΔT_{on}	*s*	11.29	15.74	19.41	16.85	1.11	7
# of Y_1-Y_3 Firing Cycles	-	-	6	9	10	4	40
# of Y_2-Y_4 Firing Cycles	-	-	24	30	31	7	21
# of Z_1 Firing Cycles	-	-	4	6	3	1	40
# of Z_2 Firing Cycles	-	-	13	26	25	12	49
# of Z_3 Firing Cycles	-	-	59	63	63	4	6
# of Z_4 Firing Cycles	-	-	25	43	43	18	42
ΔV_x in Body Frame	*mm/s*	0.00	0.00	-0.01	0.01	0.01	100
ΔV_y in Body Frame	*mm/s*	0.00	0.00	-0.01	-0.02	0.02	100
ΔV_z in Body Frame	*mm/s*	-3.56	-4.96	-6.59	-5.73	0.76	13
ΔV (Magnitude)	*mm/s*	3.56	4.96	6.59	5.73	0.76	13
Consumed Hydrazine Mass	*grams*	10.2	12.3	13.8	13.0	0.7	6

Table 3.h Comparing Results for RWA Bias Event on March 29, 2010

RWA Bias Event: 03/29/2010 (DOY 088) Thrust = 0.75 N		GSW (Ideal)	GSW	FSDS Simulation	Flight Data	Abs. Diff. Flight – GSW	%Abs. Diff. (per Flight)
Initial RWA Rates	*RPM*	[-722, -1008, -364]				-	-
Final RWA Rates	*RPM*	[-526, -1060, -442]				-	-
Bias Size (RWA Rate Change)	*RPM*	[+196, -52, -78]				-	-
Bias Time Duration	*s*	190				-	-
ΔT_{on} Y_1-Y_3 Thruster Pair	*s*	0.21	0.20	0.13	0.25	0.05	19
ΔT_{on} Y_2-Y_4 Thruster Pair	*s*	0.55	0.54	0.50	0.63	0.09	15
ΔT_{on} Z_1 Thruster	*s*	2.34	2.43	2.38	2.38	0.05	2
ΔT_{on} Z_2 Thruster	*s*	0.00	0.75	0.25	0.37	0.38	-
ΔT_{on} Z_3 Thruster	*s*	0.00	0.25	0.00	0.25	0.00	0
ΔT_{on} Z_4 Thruster	*s*	1.95	2.56	2.13	2.25	0.31	14
Total Z-Facing RCS ΔT_{on}	*s*	4.29	5.99	4.75	5.25	0.74	14
# of Y_1-Y_3 Firing Cycles	-	-	1	1	2	1	36
# of Y_2-Y_4 Firing Cycles	-	-	3	3	5	2	31
# of Z_1 Firing Cycles	-	-	16	12	18	2	14
# of Z_2 Firing Cycles	-	-	5	2	3	2	60
# of Z_3 Firing Cycles	-	-	2	0	2	0	20
# of Z_4 Firing Cycles	-	-	16	10	17	1	4
ΔV_x in Body Frame	*mm/s*	0.00	0.00	0.00	-0.01	0.01	100
ΔV_y in Body Frame	*mm/s*	0.00	0.00	0.00	-0.01	0.01	100
ΔV_z in Body Frame	*mm/s*	-1.36	-1.89	-1.58	-1.72	0.17	10
ΔV (Magnitude)	*mm/s*	1.36	1.89	1.58	1.72	0.17	10
Consumed Hydrazine Mass	*grams*	2.8	3.6	2.6	2.6	1.0	39

IX. Summary and Conclusions

Cassini continues its successful mission conducting scientific investigations of Saturn and its rings and satellites. Cassini's four-year prime mission ended in 2008, but this sophisticated spacecraft has extended its mission by additional 9 years and is about to complete its two-year Equinox extended mission.

The use of the RCS thrusters often imparts undesired ΔV on the spacecraft. The navigation requires that the spacecraft system provides predictions of ΔV in spacecraft and EME-2000 inertial coordinates resulting from a reaction wheel bias event. It is crucial for both Cassini spacecraft attitude control and navigation teams to be able to, quickly but accurately, predict the hydrazine usage and ΔV for key reaction wheel bias events, without actually having to spend time and resources simulating the event in FSDS or hardware-in-the-loop simulation environments.

This paper explains an innovative methodology for accurate and flight-calibrated determination of the RCS thruster on-times, without any form of simulation, for reaction wheel biases. The hydrazine usage and the ΔV vector in both spacecraft body frame and EME-2000 inertial frame are also computed from the thruster on-times. The algorithms within this methodology are implemented in a ground software tool. This methodology assumes a priori knowledge of thrust magnitude and thruster pulse rise and tail time constants for individual RCS thrusters, as well as the spacecraft's wet mass and center of mass location in body frame. In spite of many challenges in determining thruster on-times which results from the bang-off-bang RCS thruster controller characteristics, this methodology generates results that match with flight results with adequate accuracy. When averaged over a sample of eight bias events, the average difference of on-times between the flight data and the output of this methodology is less than 0.6 s, the average difference in Z-axis ΔV is less than 0.8 mm/s, and the average difference in hydrazine mass is less than 1.1 grams.

Acknowledgements

The work described in this paper was carried out by Jet Propulsion Laboratory, California Institute of Technology, under a contract with the National Aeronautics and Space Administration. Reference to any specific commercial product, process, or service by trade name, trademark, manufacturer, or otherwise, does not constitute or imply its endorsement by the United States Government or the Jet Propulsion Laboratory, California Institute of Technology. The methodologies and the ground software tools described in this paper have been reported to the Patent Counsel Office of Jet Propulsion Laboratory for patent application. The author is indebted to Thomas Burk, the Product Delivery Manager of the Cassini Attitude and Articulation Control Subsystem team, for the review of this paper in addition to expert discussions and critiques. The inputs and helpful suggestions from Clifford Lee and other colleagues are greatly appreciated. The author is also grateful to Cassini management for its guidance and support. Additional thanks go to Sima Lisman, the Guidance and Control Systems Engineering Group Supervisor for improving on the technical accuracy of this paper through her careful proofreading. Any remaining factual or interpretation errors are of course the author's own responsibility.

References

[1]Sarani. S., "Enceladus Plume Density Modeling and Reconstruction for Cassini Attitude Control System," SpaceOps 2010, April 25–30, 2010, Paper 2010-2035.

[2]Sarani, S., "Titan Atmospheric Density Reconstruction Using Cassini Guidance, Navigation, and Control Data," Paper AIAA 2009-5763, Proceedings of the AIAA Guidance, Navigation, and Control Conference, August 10–13, Chicago, Illinois, 2009.

[3]Sarani, S., "A Novel Methodology for Reconstruction of Titan Atmospheric Density Using Cassini Guidance, Navigation, and Control Data," Paper AIAA 2007-6343, Proceedings of the AIAA Guidance, Navigation, and Control Conference, August 20–23, Hilton Head, South Carolina, 2007.

[4]Brown, C.D., *Spacecraft Propulsion,* AIAA Education Series, American Aeronautics and Astronautics, Inc., Washington, D.C., 1996, pp. 44-50.

[5]Barber, T.J. and Cowley, R.T., "Initial Cassini Propulsion System In-Flight Characterization," AIAA-2002-4152. *38th AIAA/ASME/SAE/ASEE Joint Propulsion Conference and Exhibit*, Indianapolis, Indiana, 2002.

[6]Wong, E. and Breckenridge, W., "An Attitude Control Design for the Cassini Spacecraft," *Proceedings of the AIAA Guidance, Navigation, and Control Conference*, AIAA, Washington, DC, 1995.

[7]Chiang, R.Y., Breckenridge, W.G., and Wong, E., "Self-tuning Thruster Control for Cassini Spacecraft," *Proceedings of the AIAA Guidance, Navigation, and Control Conference*, San Diego, California, July 28-31, 1996.

[8]Lee, A. Y. and Hanover, G. "Cassini Spacecraft Attitude Control System Flight Performance," *Proceedings of the AIAA Guidance, Navigation, and Control Conference*, San Francisco, California, August 15-18, 2005.

[9]Enright, P., and Wong, E. C., "Propellant Sloshing Models for the Cassini Spacecraft," AIAA Paper 94-3730, 1994.

[10]Enright, P. and Macala, G.A., "Attitude and Articulation Control of the CRAF/Cassini Spacecraft in the Presence of Structural Flexibilities and Propellant Slosh," *Proceedings of the 15th Annual AAS Guidance and Control Conference*, Keystone, Colorado, February 8-12, 1992.

[11]Macala, G.A., "Design of the Reaction Wheel Attitude Control System for the Cassini Spacecraft," Paper AAS 02-121, *AAS/AIAA Space Flight Mechanics Meeting*, San Antonio, Texas, January 27-30, 2002.

[12]Brown, J., Lam, D., Burk, T., and Wette, M., "The Role of the Flight Software Development System Simulator Throughout the Cassini Mission," *Proceedings of the AIAA Guidance, Navigation, and Control Conference, and Exhibit*, San Francisco, California, August 15-18, 2005.

[13]Lee, A.Y. and Wertz, J.A., "In-Flight Estimation of the Cassini Spacecraft's Inertia Tensor," *Journal of Spacecraft and Rockets*, Vol. 39, No. 1, January-February 2002, pp. 153-154.

[14]Sarani, S., "Assessment of Per-Axis Thruster Control Authority of Cassini Spacecraft for Low Altitude Titan Flybys," Paper AAS 04-275, *14th AAS/AIAA Space Flight Mechanics Conference*, Maui, Hawaii, February 8-12, 2004, pp. 4-6.

[15]Bates. D., "Cassini Spacecraft In-Flight Swap To Backup Attitude Control Thrusters," Proceedings of the AIAA Guidance, Navigation, and Control Conference, August 2–6, Toronto, Canada, 2010.